

Microwave Spectrum and Structure of the Acetylene–OCS Dimer

Sean A. Peebles and Robert L. Kuczkowski*

Department of Chemistry, The University of Michigan, Ann Arbor, Michigan 48109-1055

Received: February 3, 1999; In Final Form: March 24, 1999

The rotational spectra of four isotopomers of the HCCH–OCS van der Waals dimer have been observed with a Fourier transform microwave spectrometer. The rotational constants for the normal isotopomer were determined to be $A = 5839.1071(20)$ MHz, $B = 2055.4388(13)$ MHz, and $C = 1514.9785(12)$ MHz. The rotational constants are consistent with a nearly parallel arrangement of the monomer subunits with a calculated R_{CM} distance of $3.6062(13)$ Å. A semiempirical model employing electrostatic, dispersion, and repulsion interactions was used to study the structure and binding of the system and reproduced the geometry of the dimer successfully. Comparisons with the model results for the closely related HCCH–CO₂ and HCCH–N₂O systems will also be presented.

Introduction

Recent studies of the trimer systems CO₂–CO₂–OCS,^{1,2} OCS–OCS–CO₂,³ and CO₂–CO₂–N₂O⁴ have indicated that the use of a semiempirical model can be of significant benefit to the experimentalist. In the above trimer systems and in the dimer systems of SO₂–OCS⁵ and SO₂–CS₂,⁶ the ORIENT model⁷ has been used to predict possible structures in advance of the experimental searches. In the case of the trimers of linear triatomic monomers, the agreement between the model and the experimental structures was seen to be somewhat better than in the SO₂-containing complexes. However, even in the SO₂ complexes, the model proved to be useful in terms of allowing the examination of possible structures and their relative energies, prior to embarking on the search for their spectra.

To continue the study of trimers that are comprised of linear monomers, it is necessary to ensure that the corresponding dimer structures are well-known. This allows not only a better understanding of the likely geometries of the trimers but also makes possible comparisons between the dimer structures in the isolated dimers and in the dimer portion within a trimer. From these subtle structural differences, it should be possible to observe the effects of a third body, and ultimately, it is hoped that we will be able to understand and quantify these effects as studies are extended to larger clusters. Trimers containing HCCH and OCS would be an attractive possibility, allowing us to look for similarities between the trimers of HCCH–OCS with those of CO₂–OCS.^{1–3} The first step in such a study is to ensure that the structure HCCH–OCS is determined and understood, a system that, until now, had not been characterized by high-resolution spectroscopy.

In this paper we report on the analysis of the rotational spectrum of four isotopomers of the HCCH–OCS complex. A structure in which the two monomers lie almost parallel to each other has been determined from least-squares-fitting the moments of inertia. This type of parallel structure is fairly typical of HCCH complexes and has been seen in both HCCH–N₂O⁸ and HCCH–CO₂.⁹

The ORIENT model mentioned above employs electrostatic, dispersion, and repulsion interactions and was used to reproduce

the experimental structure and to gain insight into the nature of the structure and binding in this complex. Some exploration of the performance of the model with slightly different parameters was also carried out to try to improve the agreement between prediction and experiment. The model was also applied to the HCCH–CO₂ and HCCH–N₂O systems to see whether it performs consistently with complexes containing HCCH.

Experimental Section

The rotational spectra of the HCCH–OCS dimer and three additional isotopomers were measured with a Balle–Flygare Fourier transform microwave spectrometer in the frequency range 5.5–15 GHz. The autoscanner capability of the University of Michigan FTMW spectrometer enabled an initial search to be made over a 1.3 GHz region between 6.5 and 7.8 GHz, and this search revealed a large number of transitions. Careful mixing experiments eliminated transitions that did not require both components, and Stark effect measurements were carried out on any strong lines that remained. Only six of the many lines that had been found in the initial search region turned out to be due to the HCCH–OCS dimer. Stark effect experiments were carried out by the application of an electric field up to ± 8 kV to a pair of stainless steel mesh plates measuring approximately 50 cm \times 50 cm that are situated above and below the Fabry–Perot cavity and separated by some 30 cm. Calibration of the electric field was carried out daily by measurement of the $1 \leftarrow 0$ transition of OCS at 12162.980 MHz, assuming a dipole moment of 0.7152 D.¹⁰

The HCCH–OCS dimer was generated in a supersonic expansion of a gas mixture of approximately 1.5% of each of the two components diluted in a “first run” He–Ne carrier gas (90% Ne, 10% He) at a backing pressure of ca. 2.7 atm. The gas mixture was expanded into the evacuated cavity through a modified Bosch fuel injector valve, in a direction perpendicular to the resonator axis. This alignment dramatically reduces Doppler doubling and results in a line with full width at half-maximum of the order of 30 kHz. Transition frequencies were reproducible to within 2 kHz. The more intense lines for the normal species were easily visible in 100 shots with signal-to-noise ratios in excess of 20. To resolve the small nuclear quadrupole hyperfine splittings in the DCCD–OCS isotopomer,

* Corresponding author.

TABLE 1: Observed Rotational Transitions for the Normal Species of HCCH–OCS

$J_{K_a K_c}'$	$J_{K_a K_c}''$	$\nu_{\text{obs}}/\text{MHz}$	$\Delta\nu/\text{kHz}^a$
1 ₁₁	0 ₀₀	7354.0675	0.4
2 ₁₂	1 ₁₁	6600.2781	0.0
2 ₀₂	1 ₀₁	7086.7494	−0.3
2 ₁₁	1 ₁₀	7680.8134	1.9
2 ₁₂	1 ₀₁	10383.9613	−1.3
2 ₂₀	2 ₁₁	11404.3594	5.7
2 ₂₁	2 ₁₂	12971.4021	−5.5
3 ₁₂	3 ₀₃	5904.5938	1.7
3 ₀₃	2 ₁₂	7201.3885	0.7
3 ₁₃	2 ₁₂	9867.9895	1.4
3 ₀₃	2 ₀₂	10498.6013	0.6
3 ₂₂	2 ₂₁	10710.2511	8.5
3 ₂₁	2 ₂₀	10921.9512	−4.5
3 ₁₂	2 ₁₁	11485.1180	−1.1
3 ₁₃	2 ₀₂	13165.1997	−1.2
3 ₂₂	3 ₁₃	13813.6642	2.1
4 ₁₃	4 ₀₄	7374.9007	1.9
4 ₀₄	3 ₁₃	11104.4552	−1.9
4 ₁₄	3 ₁₃	13101.3170	−3.7
4 ₀₄	3 ₀₃	13771.0569	−0.4
4 ₂₃	3 ₂₂	14237.5511	−0.9
4 ₂₂	3 ₂₁	14745.7664	0.3
5 ₁₄	4 ₂₃	9353.8956	2.4
5 ₁₄	5 ₀₅	9397.2323	−3.0

$$^a \Delta\nu = \nu_{\text{obsd}} - \nu_{\text{calcd}}$$

increased resolution was attained by the use of an axial nozzle. The gas mixture was expanded through a General Valve Corporation series 9 pulsed valve situated just off-center in one of the Fabry–Perot mirrors. Line widths were substantially reduced to ca. 10 kHz, and a Doppler doubling of 30–50 kHz (dependent on the particular frequency) was observed. This higher resolution allowed the assignment of nuclear hyperfine components to be made for several transitions of the DCCD–OCS isotopomer where the hyperfine splittings typically extended over a region of only 100–200 kHz, making resolution difficult even with the improved resolution offered by the axial nozzle.

The HCCH–OC³⁴S isotopomer was observed in natural abundance (ca. 4%). Some of the stronger *b*-type transitions for this species were visible in signal-to-noise ratios in excess of 10 in 500 shots, although lines often required averaging for a couple of thousand shots in order to achieve acceptable signal-to-noise. The HCCH–¹⁸OCS isotopomer was observed using an isotopically enriched sample of ¹⁸OCS (93.4% ¹⁸O, Isotec).

The DCCD–OCS isotopomer was observed using isotopically enriched DCCD purchased from MSD Isotopes (98% D).

A number of transitions that required both HCCH and OCS that were discovered in the initial search region still remain unassigned, and attempts to assign these to one of the two possible mixed trimer systems (OCS–OCS–HCCH or HCCH–HCCH–OCS) or to another isomer of HCCH–OCS are currently underway.

Results

I. Spectra. Both *a*- and *b*-type transitions were observed for all isotopomers, with the *b*-type transitions being the most intense. Searches for *c*-type transitions proved to be unsuccessful. The absence of *c*-type transitions suggests an *ab* plane of symmetry, and hence, a planar complex is the most likely. Transition frequencies for the 24 observed lines for the normal isotopomer are listed in Table 1. Transition frequencies for the other three isotopomers are available as Supporting Information. The spectroscopic constants obtained from a fit of these transitions to a Watson *A* reduction Hamiltonian in the *I'* representation¹¹ are given in Table 2, along with the fitted constants for the additional three isotopomers. Isotopic shifts calculated using a model that was obtained from a semiempirical model calculation (to be discussed in the Discussion) enabled quick location of the additional isotopomers.

II. Dipole Moment. Observed Stark coefficients for eight components from five rotational transitions were least-squares-fitted to determine the dipole moment components for the HCCH–OCS dimer. The fitted dipole components were found to be $\mu_a = 0.2011(5)$ D and $\mu_b = 0.6259(8)$ D, leading to a total dipole moment, μ_{total} , of 0.6574(8) D. The total dipole moment is within 0.06 D of the OCS monomer moment of 0.7152 D.¹⁰ The observed and calculated Stark coefficients are given in Table 3.

III. Structure. The absence of *c*-type transitions for this complex suggests that the structure is probably planar. Calculation of the inertial defect, Δ , for the normal species gives a value of 1.163 u Å². This is slightly larger than the inertial defects observed in other planar acetylene complexes such as HCCH–N₂O⁶ ($\Delta = 0.841$ u Å²), HCCH–H₂CO¹² ($\Delta = 0.643$ u Å²), and HCCH–CO₂⁸ ($\Delta = 0.80$ u Å²) but is still small enough that, taken along with the small centrifugal distortion constants, it provides evidence that the complex is reasonably rigid. The value of Δ can be seen to change very little upon isotopic substitution (Table 2), with all four isotopomers having

TABLE 2: Spectroscopic Constants for the Four Isotopomers of HCCH–OCS

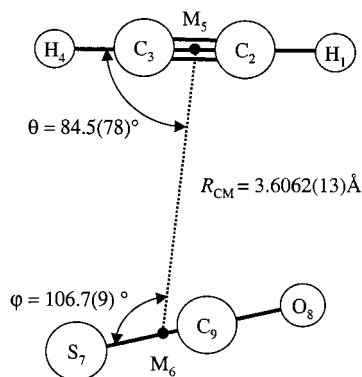
spectroscopic constant	HCCH–OCS	HCCH– ¹⁸ OCS	HCCH–OC ³⁴ S	DCCD–OCS
<i>A</i> /MHz	5839.1071(20)	5489.6306(28)	5761.4525(22)	5487.5615(22)
<i>B</i> /MHz	2055.4388(13)	2053.5079(42)	2018.8491(27)	1963.6641(12)
<i>C</i> /MHz	1514.9785(12)	1489.2072(39)	1489.8421(25)	1441.3160(18)
Δ_J/kHz	8.69(2)	8.50(7)	8.27(5)	7.78(5)
Δ_{JK}/kHz	2.9(1)	3.3(3)	1.5(3)	6.51(10)
Δ_K/kHz	44.3(4)	36.5(7)	46.8(5)	28.2(7)
δ_J/kHz	2.527(8)	2.59(1)	2.43(2)	2.30(4)
δ_K/kHz	28.2(6)	26.2(19)	23.1(13)	23.1(5)
$\chi_{aa}^{(1)}/\text{MHz}$				−0.075(10)
$\chi_{bb}^{(1)}/\text{MHz}$				0.150(10)
$\chi_{aa}^{(2)}/\text{MHz}$				−0.100(10)
$\chi_{bb}^{(2)}/\text{MHz}$				0.212(10)
$\Delta/\text{u Å}^2$	1.163	1.195	1.169	1.176
$P_{cc}/\text{u Å}^2$	−0.582	−0.598	−0.584	−0.588
$\Delta\nu_{\text{rms}}/\text{kHz}^b$	2.96	2.90	2.51	2.68
<i>N</i> ^c	24	21	18	38

^a Inertial defect, $\Delta = (I_c - I_a - I_b)$. ^b $\Delta\nu_{\text{rms}} = [\sum(\nu_{\text{obsd}} - \nu_{\text{calcd}})^2/N]^{1/2}$. ^c *N* is the number of fitted transitions.

TABLE 3: Stark Coefficients and Dipole Moment Components for HCCH–OCS

transition	$ M $	$\Delta\nu/\epsilon^2$ ^a	obsd – calcd ^a
1 ₁₁ –0 ₀₀	0	6.2912	0.0024
2 ₀₂ –1 ₀₁	0	2.5439	–0.0104
	1	6.5391	–0.0464
2 ₁₂ –1 ₁₁	1	6.7339	–0.0017
2 ₁₁ –1 ₁₀	1	–8.6004	–0.0032
4 ₁₃ –4 ₀₄	2	1.3799	0.0201
	3	3.0508	0.0181
	4	5.4157	0.0409
	$\mu_a = 0.2011(5)$ D		
	$\mu_b = 0.6259(8)$ D		
	$\mu_c = 0.00(5)$ D ^b		
	$\mu_{\text{tot}} = 0.6574(8)$ D		

^a Observed Stark coefficients and residuals are in units of 10^{-4} MHz/(V cm^{–1}). ^b μ_c fixed at zero during fitting.

**Figure 1.** Structure of the HCCH–OCS complex in the *ab* symmetry plane showing the definition of the fitted structural parameters and the atom numbering scheme.

values in the range 1.18 ± 0.02 u Å². Positive values of Δ usually arise from Coriolis interactions from in-plane vibrational modes.

Further evidence in favor of a planar geometry may be obtained by inspection of the rotational constant *A* for the normal species. We can use the following expression to estimate the value of *A* that would be expected if the two monomers were aligned parallel to each other,

$$\frac{1}{A(\text{complex})} = \frac{1}{B_0(\text{HCCH})} + \frac{1}{B_0(\text{OCS})} \quad (1)$$

where *A* is the measured rotational constant for the HCCH–OCS complex and *B*₀(HCCH) and *B*₀(OCS) are the rotational constants for free HCCH (*B*₀(HCCH) = 35273.8 MHz¹³) and OCS (*B*₀(OCS) = 6081.19 MHz¹⁴). This expression gives a value of *A* of 5186.96 MHz, within 11% of the experimental value of 5839.11 MHz, and suggests that the two monomers are likely aligned close to parallel to each other.

The moments of inertia for the normal species and the three additional isotopomers allowed a least-squares fitting to the three structural parameters required to describe the structure of this dimer, the *R*_{CM} distance, the angle θ (the C₃–M₅···M₆ angle), and the angle φ (S₇–M₆···M₅). The centers M₅ and M₆ are the centers of mass of the acetylene and the OCS, respectively; all atom numbering is defined in Figure 1. The University of Michigan implementation of the STRFTQ program of Schwendeman was used in the fitting of the inertial data. Owing to the relatively large nonzero inertial defect, a fit of all three moments of inertia for the four isotopomers will result in a large standard deviation for the fit. For this reason, experimentation with the

TABLE 4: Principal Axis Coordinates for the Fitted Structure of HCCH–OCS^a

atom	<i>a</i>	<i>b</i>	<i>c</i>
H ₁	2.896 44	1.225 15	0.000 00
C ₂	2.634 08	0.197 10	0.000 00
C ₃	2.336 61	–0.968 55	0.000 00
H ₄	2.074 25	–1.996 60	0.000 00
M ₅	2.485 35	–0.385 72	0.000 00
M ₆	–1.078 23	0.167 33	0.000 00
S ₇	–1.526 52	–0.769 99	0.000 00
	[1.506 42]	[0.785 03]	0.000 00
O ₈	–0.352 43	1.684 89	0.000 00
	[0.348 97]	[1.681 13]	0.000 00
C ₉	–0.851 24	0.641 94	0.000 00

^a Values in brackets for the S and O atoms are the coordinates obtained from the Kraitchman single isotopic substitution calculations. All coordinates are given in angstroms.

fitting program revealed that only *I*_a and *I*_c should be fit for each isotopomer to try to offset the nonzero inertial defect. The principal axis coordinates that result from this least-squares fitting are listed in Table 4 with the corresponding structural parameters given in Table 5. The monomer structures were assumed to be unchanged in the dimer during the fitting process (*r*(C≡C) = 1.203 Å and *r*(C–H) = 1.061 Å in acetylene¹⁵ and *r*(C=O) = 1.1561 Å and *r*(C=S) = 1.5651 Å in OCS¹⁵). Also listed in Table 4, where available, are the coordinates from the Kraitchman single isotopic substitution calculations.¹⁶ Inertial data for the singly substituted ¹⁸OCS and the OC³⁴S isotopomers enabled the principal axis coordinates of the OCS molecule to be calculated and hence the orientation of the OCS with respect to the principal axes to be determined. The O–S distance in OCS calculated from the Kraitchman coordinates determined for these atoms is 2.7243 Å, in excellent agreement with the 2.7212 Å obtained by using the literature monomer geometry.¹⁵ The fitted parameters were found to be *R*_{CM} = 3.6062(13) Å, θ = 84.5(78)°, and φ = 106.7(9)° with a ΔI_{rms} value of 0.358 u Å² and are illustrated in Figure 1. The uncertainties in the parameters are statistical uncertainties (1 σ) that result from the fitting program. The structural parameters may be considered to describe an effective ground-state structure, and we expect the equilibrium values to fall within approximately 0.05 Å for the center-of-mass separation, 5° for θ and 10° for φ .

The fitted structure from the inertial data was used to estimate dipole moments for the complex based on a simple projection of the OCS monomer dipole moment¹⁰ onto the principal axis frame of the dimer. This leads to values of μ_a = 0.31 D and μ_b = 0.65 D, close to the values that result from the experimental determination. This suggests that polarization effects are not particularly significant, since induced dipole contributions are reasonably small. Calculations that include polarization effects will be described in the Discussion.

IV. Deuterium Nuclear Quadrupole Coupling Constants.

As described in the Experimental Section, some of the nuclear quadrupole hyperfine splittings in the DCCD–OCS isotopomer were resolvable. The individual splittings were small, of the order of a few tens of kilohertz at best, but careful inspection of the Doppler doublets and a comparison with predictions in which the nuclear quadrupole coupling constants of the DCCD monomer¹⁷ were projected into the principal axis frame of the structure obtained from the inertial fit (giving χ_{aa} = –0.087 MHz and χ_{bb} = 0.199 MHz) allowed an assignment of the components to be made. A total of 38 hyperfine components from 8 transitions were measured. Global fits of rotational, centrifugal distortion constants, and nuclear quadrupole coupling

TABLE 5: Structural Parameters, Rotational Constants, and Dipole Moment Components for HCCH–OCS from Experiment and Predictions from the ORIENT Model

parameter	exptl	ORIENT (no induction) $K = 0.001 E_h$	ORIENT (no induction) $K = 0.001 375 E_h$	ORIENT (+ induction) $K = 0.001 E_h$	ORIENT (+ induction) $K = 0.001 55 E_h$
$R_{CM}/\text{\AA}$	3.6062(13)	3.424	3.603	3.367	3.603
θ/deg	84.5(78)	84.7	86.3	82.6	84.6
φ/deg	106.7(9)	107.6	107.6	107.3	107.3
$\Delta I_{rms}^a/\text{u \AA}^2$	0.358				
A/MHz	5839.1071	5947.893	5889.112	5965.975	5878.472
B/MHz	2055.4388	2245.678	2045.731	2315.086	2046.516
C/MHz	1514.9785	1630.187	1518.308	1667.872	1518.032
μ_a/D	0.2011	0.36	0.34	0.14	0.03
μ_b/D	0.6259	0.67	0.68	0.55	0.58

^a ΔI_{rms} is the standard deviation of the fit.

TABLE 6: Distributed Multipoles for HCCH and OCS^a

atom	z^b	Q_{00}	Q_{10}	Q_{20}	Q_{30}	Q_{40}
H	3.141 67	0.033 24	0.304 54	-0.132 57	0.069 60	-0.046 14
C	1.136 67	-0.033 24	0.422 91	-0.302 30	-1.603 27	2.115 96
C	-1.136 67	-0.033 24	-0.422 91	-0.302 30	1.603 27	2.115 96
H	-3.141 67	0.033 24	-0.304 54	-0.132 57	-0.069 60	-0.046 14
C	0.000 00	0.645 86	-0.458 33	0.287 38	1.753 20	7.087 56
O	-2.184 71	-0.519 07	-0.083 49	0.276 77	0.436 94	0.708 45
S	2.957 61	-0.126 79	0.080 06	1.659 44	-0.774 81	2.340 81

^a All quantities are in atomic units. ^b z coordinate of the atom in bohr.

constants were not possible with this particular mixture of lines. Attempts to fix everything except the four nuclear quadrupole coupling constants (χ_{aa} and χ_{bb} for the two deuterium nuclei) also led to a failure to fit, with the values of χ_{aa} for the two deuterium nuclei oscillating and failing to converge. Fits in which the coupling constants were fitted individually were tried, and the resulting values fed back into the program in an iterative process. The rotational and distortion constants were then fitted to give the values listed in the final column of Table 2, with a standard deviation of 2.68 kHz. Variation of the values of the derived coupling constants allowed us to estimate the uncertainties and to ensure that the fit was reasonable.

Comparison of the fitted coupling constants with the values obtained by projection of the monomer constants onto the principal axis frame of the dimer shows that the structure is consistent with the coupling constants. Clearly, the environments of the two deuterium atoms are different enough that noticeably different nuclear quadrupole coupling constants for the two sites might arise. This is not surprising given that similar differential effects were observed in the nitrogen coupling constants of HCCH–N₂O.⁸

Discussion

A semiempirical model was employed during the initial modeling of this complex to explore possible structures and to allow predictions of the spectrum to guide the searches. The ORIENT model⁷ of Anthony Stone was used with distributed multipole moments (DMM's) calculated with the CADPAC suite of programs¹⁸ at the SCF level with a TZ2P basis from the CADPAC library. Multipoles up to and including hexadecapoles were calculated at the atomic centers; the DMM's for acetylene and OCS are listed in Table 6. In addition to the electrostatic interaction that is afforded by the DMM's, dispersion and repulsion interactions were included in the intermolecular interaction potential by means of combined dispersion–repulsion atom–atom parameters of the exp–6 form. In this formulation the combined dispersion–repulsion contribution to the interaction energy for an interaction between two molecules

A and B may be given by¹⁹

$$U_{\text{exp-6}} = \sum_{ij} K \exp[-\alpha_{ij}(R_{ij} - \rho_{ij})] - \frac{C_6^{ij}}{R_{ij}^6} \quad (2)$$

where K is an energy unit that is taken to be $0.001 E_h$ (hartree) by default and allows fine-tuning of the repulsion portion of the potential. R_{ij} is the separation between sites i and j in the molecules A and B, respectively. α_{ij} is a measure of the hardness of the exponential repulsion, ρ_{ij} is a sum of effective radii of the sites i and j , and C_6^{ij} is an empirical site–site dispersion term. Values for α_{ij} , ρ_{ij} , and C_6^{ij} were taken from the tabulated values of Mirsky²⁰ in Table 11.2 of ref 19. Values for atom–atom pairs not available in ref 19 were generated by means of the following approximate combining rules: harmonic mean for α (i.e., $1/\alpha_{ij} \approx 1/\alpha_i + 1/\alpha_j$), geometric mean for C_6 , and arithmetic mean for ρ .

The global minimum structure (-641.6 cm^{-1}) that resulted from the ORIENT model with the default parameters was very similar in appearance to the structure from the inertial fit. Table 5 compares the values of the parameters R_{CM} , θ , and φ , and it can be seen that in the case of the angles, agreement between the experimental and calculated values is excellent. The R_{CM} distance is underestimated quite considerably by the model, being some 0.18 \AA too short. Increasing the value of the preexponential factor K to $0.001 375 E_h$ brings the R_{CM} distance into quantitative agreement with the experimental value and changes the other parameters by very little (see the third column in Table 5). A comparison of the experimental and predicted rotational constants and dipole moment components is also given in Table 5 and shows that the standard model (without induction) has performed reasonably well in this case.

In an attempt to see whether the ORIENT model predicts any significant polarization effects in this complex, we carried out a simple, low-level induction calculation. We may include a simplistic induction interaction by the addition of a molecular polarizability placed at the center of mass of each monomer. Values of the polarizabilities for HCCH²¹ ($\alpha = 3.36 \text{ \AA}^3$, $\gamma = 1.75 \text{ \AA}^3$) and OCS²² ($\alpha = 5.21 \text{ \AA}^3$, $\gamma = 4.67 \text{ \AA}^3$) were taken from the tables in ref 23. The induction energy and the calculation of the induced moments are then iterated to convergence. The resulting structure (using the default value of $K = 0.001 E_h$) shows very little change from the calculation in which induction was neglected. R_{CM} is reduced as would be expected by the addition of another attractive contribution, and the angles θ and φ are within 2° or so of the values from the calculation with default parameters without induction. The dipole moment components of $\mu_a = 0.14 \text{ D}$ and $\mu_b = 0.55 \text{ D}$ include

TABLE 7: Distributed Multipoles for CO₂ and N₂O^a

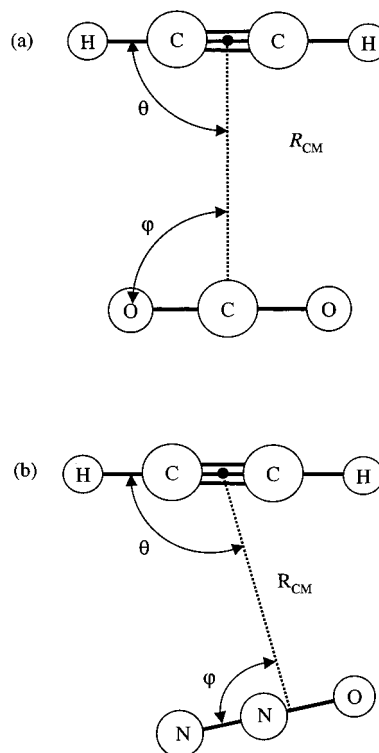
atom	z^b	Q_{00}	Q_{10}	Q_{20}	Q_{30}	Q_{40}
C	0.000 00	1.397 50	0.000 00	-0.277 26	0.000 00	1.910 77
O	2.195 86	-0.698 75	0.394 87	-0.168 80	0.286 94	-0.222 64
O	-2.195 86	-0.698 75	-0.394 87	-0.168 80	-0.286 94	-0.222 64
N	0.000 00	0.626 01	0.454 67	0.023 98	-0.517 85	2.391 21
N	-2.127 83	-0.134 93	0.087 86	-0.065 68	0.368 81	0.927 93
O	2.250 66	-0.491 09	0.004 39	0.496 16	0.372 22	-0.735 13

^a All quantities are in atomic units. ^b z coordinate of the atom in bohr.

corrections for induced moments and are slightly smaller than the values that result in the calculation with no induction included ($\mu_a = 0.36$ D and $\mu_b = 0.67$ D). Adjustment of the preexponential factor K to a value of $0.001\ 55 E_h$ was necessary to reproduce the experimental R_{CM} value; the parameters for this structure are given in the last column of Table 5 along with the resulting rotational constants and dipole moment components. It can be seen from the table that the rotational constants are not very different from the calculation with no induction and in which a value of K of $0.001\ 375 E_h$ was used. The μ_a dipole component is approximately zero and has been overcorrected by the inclusion of polarization, but the μ_b component remains at around 0.58 D. The tendency of the μ_a component (and to a smaller extent the μ_b component) to be reduced upon inclusion of polarization effects in the model is consistent with the measured moments being slightly less than the projected dipole moments obtained from the inertial fit structure (see Structure in Results).

In addition to modeling the HCCH–OCS complex, the two closely related complexes HCCH–CO₂ and HCCH–N₂O were modeled using the same approach as for HCCH–OCS. Values for the polarizabilities of CO₂²¹ ($\alpha = 2.59 \text{ \AA}^3$, $\gamma = 2.03 \text{ \AA}^3$) and N₂O²¹ ($\alpha = 2.93 \text{ \AA}^3$, $\gamma = 2.83 \text{ \AA}^3$) were taken from the tables in ref 23. Distributed multipole moments were calculated at the same SCF/TZ2P level as for HCCH and OCS, and these moments are tabulated in Table 7. Table 8 lists the calculated structural parameters for the HCCH–CO₂ complex at different levels of calculation and compares them with the experimental values (see Figure 2a for definitions of angles and distances). A value for K of $0.0013 E_h$ was required to bring the R_{CM} distance into agreement with the experimental value, and this can be seen to improve the agreement between the predicted and experimental rotational constants quite significantly. The final column in Table 8 shows little improvement in the rotational constants; since the addition of polarization effects does nothing to the angles θ and φ , they remain at exactly 90° in all of the calculations for this complex.

The HCCH–N₂O results are listed in Table 9, and its structure is shown in Figure 2b. In this case the A rotational constant is in reasonable agreement for all levels of calculation. B and C , not surprisingly, reproduce the experimental constants much

**Figure 2.** Definition of the structural parameters in the (a) HCCH–CO₂ and (b) HCCH–N₂O complexes.

more closely when the R_{CM} distance is brought closer to agreement with the experimental value by adjustment of the value of K . Again, as with HCCH–CO₂, the most important factor in the prediction of the rotational constants is seen to be how well the model predicts R_{CM} . In both calculations in which the preexponential factor, K , was varied to bring R_{CM} into agreement with the experimental value, the predicted and experimental values of the rotational constants are in very good agreement. The angles θ and φ are consistently predicted to be 99–100° and 91°, respectively, slightly larger than the assumed values of 90°. A different potential function model including electrostatic, dispersion, and repulsion energies finds that the minimum potential energy configuration of HCCH–N₂O occurs when $\theta = 90^\circ$ and $\varphi = 91^\circ$.²⁴ Furthermore, using eq 1 gives a value of A that is within 1.4% of the observed value,⁸ indicating that the angles are close to 90°. Isotopic substitution experiments may be able to refine the structure and better distinguish between the two potential functions.

Conclusions

The HCCH–OCS complex has been found to possess a structure in which the two monomers are aligned close to parallel to each other. The OCS is tilted slightly such that the O atom

TABLE 8: Comparison of Experimental and Predicted Structural Parameters and Rotational Constants for the HCCH–CO₂ Complex

parameter	exptl	ORIENT			
		(no induction) $K = 0.001 E_h$	(no induction) $K = 0.0013 E_h$	(+ induction) $K = 0.001 E_h$	(+ induction) $K = 0.0014 E_h$
$R_{CM}/\text{\AA}$	3.285	3.144	3.285	3.094	3.283
θ/deg	90 ^a	90	90	90	90
φ/deg	90 ^a	90	90	90	90
A/MHz	8876.4	8797.081	8797.081	8797.081	8797.081
B/MHz	2859.3	3126.529	2865.170	3229.971	2867.881
C/MHz	2155.3	2306.712	2161.258	2362.534	2162.800

^a The equilibrium structure of HCCH–CO₂ has C_{2v} symmetry, so the angles θ and φ are both 90°.

TABLE 9: Comparison of Predicted and Experimental Structural Parameters and Rotational Constants for the HCCH–N₂O Complex

parameter	exptl	ORIENT (no induction) $K = 0.001 E_h$	ORIENT (no induction) $K = 0.001 225 E_h$	ORIENT (+ induction) $K = 0.001 E_h$	ORIENT (+ induction) $K = 0.001 35 E_h$
$R_{CM}/\text{\AA}$	3.305	3.191	3.301	3.139	3.309
θ/deg	90 ^a	99.7	99.7	100.4	99.8
φ/deg	90 ^a	91.5	91.6	91.0	91.2
A/MHz	9394.2683	9357.913	9368.655	9343.366	9359.016
B/MHz	2831.8564	3027.934	2828.293	3130.951	2816.143
C/MHz	2168.0780	2287.703	2172.453	2345.108	2164.763

^a The angles θ and φ are assumed to be 90°. See text for discussion.

is closer to the HCCH subunit, as would be expected from a straightforward steric consideration. The C₂...C₉ and C₃...C₉ (see Figure 1) distances are found to be 3.514 and 3.572 Å, some 0.11 and 0.17 Å longer than the sum of their van der Waals radii,²⁵ respectively.

The ORIENT model performed well for this system, reproducing the angles to within less than 1° using the default parameters, although underestimating the R_{CM} distance by 0.18 Å. Experimentation with the value of the preexponential factor, K , allowed us to considerably improve the agreement of the predicted and experimental rotational constants. Addition of polarization effects also served to improve the agreement, with the calculation in which induction effects were included (and with a value of K of 0.0015 E_h) giving very good agreement with the experimental rotational constants.

For the HCCH–CO₂ and the HCCH–N₂O systems, the model (using default parameters and no induction) gave a reasonably good approximation of the structure of these complexes. The default value of K of 0.001 E_h is clearly always too small to enable a good prediction of the R_{CM} distance for these systems, resulting in R_{CM} being too short by about 0.1 Å. Inclusion of polarization effects in these cases did little to fine-tune the structure, with the most important factor in the prediction of the rotational constants being the R_{CM} distance.

The performance of the ORIENT model in the present case has been as good as or better than has been observed in recent studies of the SO₂–OCS complex⁵ and the SO₂–CS₂ complex⁶ and in a theoretical study of a variety of SO₂-containing complexes.²⁶ In these studies, some fine-tuning of the model (both by variation of the distributed multipoles and of other adjustable parameters within the model) was necessary to reproduce the experimental geometry. Even then, in some cases, such as butadiene–SO₂ and furan–SO₂,²⁵ the nature of the predicted geometry was still not in good agreement with experimental results.

It is likely that the source of at least some of the problems encountered previously has been the representation of the SO₂. In this paper, the alignment of two linear monomers seems to have presented fewer problems for the model. Further testing of the model with trimers consisting of HCCH and OCS is in progress to see whether it is able to perform as well as it did in the recent studies of CO₂–CO₂–OCS,^{1,2} OCS–OCS–CO₂,³ and CO₂–CO₂–N₂O⁴ systems. Clearly, a better representation of bent triatomics such as SO₂ needs to be formulated, whether through improved DMM descriptions or adjustment of various parameters within the model.

In summary, the model has once again proven to be useful in this study from a spectroscopic point of view. The initial guess of the structure was of sufficient quality to guide the assignment of a very sparse spectrum.

Acknowledgment. This work was supported by the Experimental Physical Chemistry Program, National Science Foundation, Washington, DC. S.A.P. expresses his thanks to Dr. Anthony Stone for much kind assistance and willingness to help with problems encountered during the transfer of the ORIENT program to our Windows NT platform.

Supporting Information Available: Tables of rotational transitions for the isotopic species. This material is available free of charge via the Internet at <http://pub.acs.org>.

References and Notes

- (1) Peebles, S. A.; Kuczkowski, R. L. *Chem. Phys. Lett.* **1998**, 286, 421.
- (2) Peebles, S. A.; Kuczkowski, R. L. *J. Chem. Phys.* **1998**, 109, 5276.
- (3) Peebles, S. A.; Kuczkowski, R. L. *J. Phys. Chem.* **1998**, 102, 8091.
- (4) Peebles, S. A.; Kuczkowski, R. L. *Mol. Phys.*, in press.
- (5) Peebles, S. A.; Kuczkowski, R. L. *J. Mol. Struct.*, in press.
- (6) Peebles, S. A.; Kuczkowski, R. L. *J. Chem. Phys.* **1999**, 110, 6804.
- (7) Stone, A. J.; Dullweber, A.; Hodges, M. P.; Popelier, P. L. A.; Wales, D. J. *ORIENT: A program for studying interactions between molecules*, version 3.2; University of Cambridge: Cambridge, U.K., 1995.
- (8) Leung, H. O. *J. Chem. Phys.* **1997**, 107, 2232.
- (9) Prichard, D. G.; Nandi, R. N.; Muentner, J. S.; Howard, B. J. *J. Chem. Phys.* **1988**, 89, 1245.
- (10) Muentner, J. S. *J. Chem. Phys.* **1968**, 48, 4544.
- (11) Watson, J. K. G. *J. Chem. Phys.* **1969**, 46, 1935.
- (12) Howard, N. W.; Legon, A. C. *J. Chem. Phys.* **1988**, 88, 6793.
- (13) Palmer, K. F.; Mickelson, M. E.; Rao, K. N. *J. Mol. Spectrosc.* **1972**, 44, 131.
- (14) Larsen, N. W.; Winnemisser, B. P. *Z. Naturforsch.* **1974**, 29a, 1213.
- (15) Harmony, M. D.; Laurie, V. W.; Kuczkowski, R. L.; Schwendeman, R. H.; Ramsay, D. A.; Lovas, F. J.; Lafferty, W. J.; Maki, A. G. *J. Phys. Chem. Ref. Data* **1979**, 8, 619.
- (16) Kraitchman, J. *Am. J. Phys.* **1953**, 21, 17.
- (17) Asdjodi, M. R.; Gregory, R. V.; Lickfield, G. C.; Spencer, H. G.; Huffman, J. W.; Savitsky, G. B. *J. Chem. Phys.* **1987**, 86, 1653.
- (18) Amos, R. D. *CADPAC: The Cambridge Analytic Derivatives Package Issue 6*; University of Cambridge: Cambridge, U.K., 1995. A suite of quantum chemistry programs developed by Amos, R. D. with contributions from the following: Alberts, I. L.; Andrews, J. S.; Colwell, S. M.; Handy, N. C.; Jayatilaka, D.; Knowles, P. J.; Kobayashi, R.; Laidig, K. E.; Laming, G.; Lee, A. M.; Maslen, P. E.; Murray, C. W.; Rice, J. E.; Simandiras, E. D.; Stone, A. J.; Su, M.-D.; Tozer, D. J.
- (19) Stone, A. J. *The Theory of Intermolecular Forces*; Clarendon Press: Oxford, 1996.
- (20) Mirsky, K. The determination of the intermolecular interaction energy by empirical methods. In *Computing in Crystallography*; Schenk, R., Olthoff-Hazenkamp, R., van Koningveld, H., Bassi, G. C., Eds.; Delft University Press: Delft, The Netherlands, 1978.
- (21) Alms, G. R.; Burnham, A. K.; Flygare, W. H. *J. Chem. Phys.* **1975**, 63, 3321.
- (22) Bogaard, M. P.; Orr, B. J. *MTP International Review of Science, Physical Chemistry, Series 2, Vol. 2. Molecular Structure and Properties*; Buckingham, A. D., Ed.; Butterworths: London, 1975; Chapter 5.
- (23) Gray, C. G.; Gubbins, K. E. *Theory of Molecular Fluids Vol. 1: Fundamentals*, Oxford University Press: Oxford, 1984.
- (24) Hu, T. A.; Sun, L. H.; Muentner, J. S. *J. Chem. Phys.* **1991**, 95, 1537.
- (25) Pauling, L. *The Nature of the Chemical Bond*, 3rd ed.; Cornell University Press: Ithaca, NY, 1960.
- (26) Peebles, S. A.; Kuczkowski, R. L. *J. Mol. Struct.* **1998**, 447, 151.